Journal of Luminescence 223 (2020) 117216

Contents lists available at ScienceDirect

Journal of Luminescence

journal homepage: http://www.elsevier.com/locate/jlumin

Recombination luminescence of X-ray induced paramagnetic defects in BaY_2F_8

Andris Antuzevics [a,*], Andris Fedotovs [a], Dzintars Berzins [a], Uldis Rogulis [a], Krisjanis Auzins [a], Aleksejs Zolotarjovs [a], Sonia Licia Baldochi [b]

[a] Institute of Solid State Physics, University of Latvia, Latvia
[b] Instituto de Pesquisas Energéticas e Nucleares, IPEN–CNEN/SP, Brazil

ARTICLE INFO

Keywords:
BaY_2F_8
Radiation defects
Recombination luminescence
Optically detected magnetic resonance (ODMR)
Electron paramagnetic resonance (EPR)

ABSTRACT

Recombination luminescence (RL) and RL-detected electron paramagnetic resonance (RL-EPR) in BaY_2F_8 single crystal has been investigated after irradiation with X-rays at low temperature. The recombination process, which lasts for several hours at 4 K, results in several broad bands in the RL spectrum. RL-EPR spectra show pronounced angular dependences on crystal orientation relative to external magnetic field. Based on the determined spin-Hamiltonian parameter values the recombination centres have been proposed to be F-type electron and self-trapped hole (V_K) centres.

1. Introduction

Monoclinic barium yttrium fluoride (BaY_2F_8) has been widely investigated as an optical material due to its high transparency, low phonon energy and low symmetry nature of the lattice. When doped with rare earth (RE) ions, BaY_2F_8 is best-known for its stimulated emission in lasers [1–11], however other applications such as scintillators [12,13], optical refrigerators [14] and up-conversion coatings for solar cells [15–18] have shown promise as well.

Efficiency of luminescence processes in materials is affected by the local structure of RE ions as well as the presence of intrinsic defects in the lattice. Although the interest in BaY_2F_8 is high, there is a relatively low number of studies focusing on the characterization of defect local structure, especially with methods, which involve magnetic resonance techniques.

The lack of magnetic resonance investigations of BaY_2F_8 can be explained by the complicated structure of the lattice, which is shown in Fig. 1. BaY_2F_8 is a monoclinic symmetry crystal (space group: C_{2h}^3-$C2/m$) with unit cell parameters $a = 6.9829$ Å; $b = 10.5190$ Å; $c = 4.2644$ Å and $\beta = 99.676°$ [19]. The local structure of cationic positions can be described in terms of YF_8 and BaF_{12} polyhedra. For fluorine ions there are three distinct sites in the primitive cell, which differ both by their symmetry as well as the occupancy factor [11].

From the RE ion family the only EPR data in BaY_2F_8 have been reported for Yb^{3+} [20]. Yb^{3+} ions are proposed to form at least three types of isolated centres and at higher doping levels – also Yb^{3+}-Yb^{3+} ion pairs. For other RE ions, such as Ce^{3+}, Nd^{3+}, Dy^{3+} and Er^{3+}, local structure peculiarities have been analysed on the basis of theoretical methods, e.g. the Newman Superposition model [21,22]. UV and X-ray induced intrinsic defects have been characterized predominantly with luminescence-based techniques [23,24]. Existence of charge traps introduce quasi-continuous distributions of energy levels in the bandgap [23]. The intrinsic defects, which are responsible for thermoluminescence peaks, are most likely F-type and V_K-type centres [24], however an unambiguous assignment would benefit from detailed studies of EPR spectra angular variations.

In this paper we report recombination luminescence (RL) of X-ray induced paramagnetic defects in BaY_2F_8. The recombination process in the long-lasting afterglow (for several hours) of a BaY_2F_8 single crystal has been investigated by measuring microwave-induced changes in the RL signal intensity. Henceforth, this method is called recombination-luminescence-detected electron paramagnetic resonance (RL-EPR) – a method allowing to detect EPR in the tunnelling RL [25]. The method is feasible only if high magnetic fields and correspondingly high microwave frequencies are available. RL-EPR spectra show pronounced dependences on BaY_2F_8 crystal orientation relative to external magnetic field. The determined spin-Hamiltonian (SH) parameters are in a good agreement with F and V_K centre values reported in higher symmetry fluoride hosts.

* Corresponding author.
E-mail address: andris.antuzevics@cfi.lu.lv (A. Antuzevics).

https://doi.org/10.1016/j.jlumin.2020.117216
Received 6 December 2019; Received in revised form 24 February 2020; Accepted 12 March 2020
Available online 12 March 2020

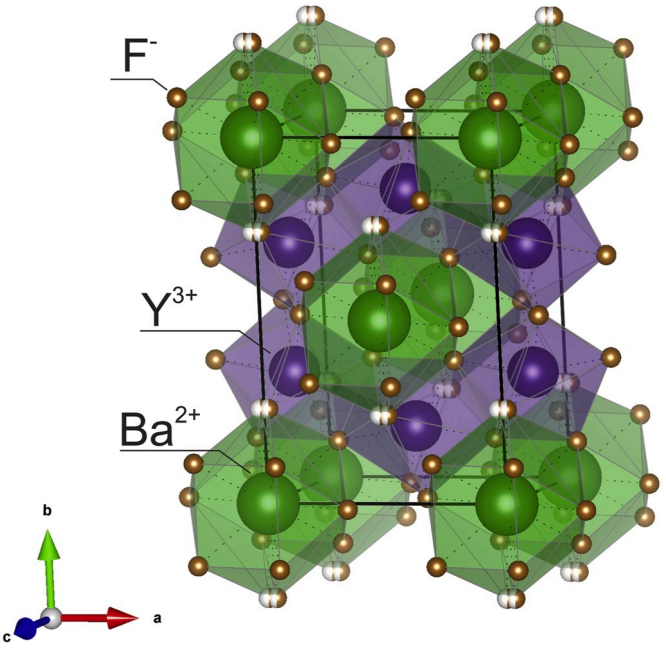

Fig. 1. Crystal structure of BaY_2F_8. Visualised in VESTA software [26] using atom coordinates obtained from Crystallography Open Database [27].

2. Experimental details

An undoped BaY_2F_8 single crystal was prepared by the zone melting method under HF atmosphere from BaF_2 and YF_3 powders following the guidelines outlined in Ref. [28].

Room temperature EPR spectra were measured with Bruker ELEXSYS-II E500 CW-EPR spectrometer operated at X-band (9.85 GHz) microwave frequency and 10 mW power. The amplitude of 100 kHz magnetic field modulation was set at 0.4 mT.

For X-ray excited luminescence, long luminescence kinetics and thermally stimulated luminescence (TSL) measurements AndorDU-401A-BV IDus CCD camera coupled with Andor Shamrock B-303i spectrograph was used. Samples were irradiated using an X-ray tube (W anode; 30 kV; 10 mA) in a helium closed-cycle cryostat (Sumitomo HC-4 with LakeShore 331 temperature controller) in a vacuum chamber (Ilmvac turbomolecular pump providing pressure lower than 10^{-5} Torr). For TSL measurements samples were irradiated for 20 min and 5-min delay was implemented after the end of irradiation to allow the afterglow to fade, a constant sample heating rate of 10 K/s was maintained for a 15–320 K range. Long kinetics measurements were performed at 10 K without delay after 20 min of irradiation, measurements were continued for 180 min with a 10 s step. Both kinetics and TSL measurements were performed using wide-open monochromator slits (2000 μm), while XRL was measured with 50 μm slits.

RL-EPR measurements, where EPR is measured in the afterglow luminescence, were performed after excitation at 4.2 K with an X-ray tube (W anode; 55 kV; 10 mA; 30 min). RL-EPR spectra were measured in the 200–900 nm spectral range with a custom-built computer-controlled spectrometer based on Oxford Instruments magneto-optical cryostat working at 62 GHz microwave frequency. RL-EPR was detected either as the integral RL intensity or in different spectral ranges using bandpass filters. For the evaluation of the resonance line positions in the RL-EPR spectra the magnetic field dependent background was subtracted.

Simulations of RL-EPR spectra angular variantions were performed in Visual-EPR software by Valentin Grachev [29], which is based on the algorithm described in Ref. [30]. Details of the simulations are given in the RL-EPR section of the article.

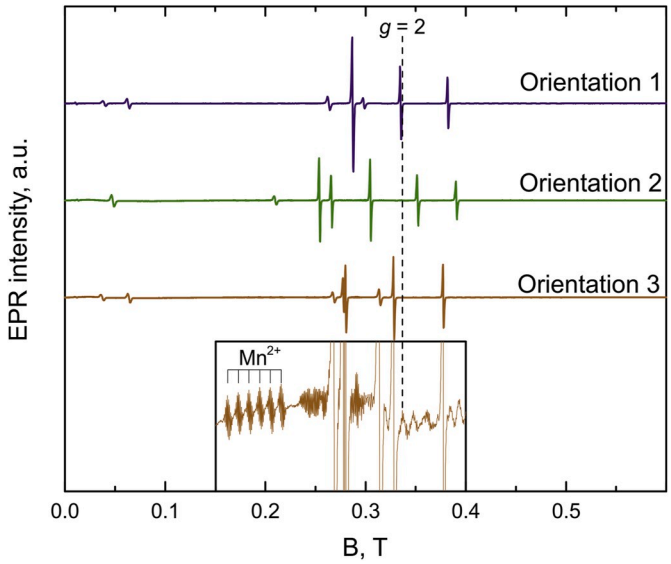

Fig. 2. Room temperature EPR spectra for different crystal orientations in respect to external magnetic field. A zoomed-in section of "Orientation 3" spectrum is shown in the inset of the figure.

3. Results and discussion

3.1. EPR

Room temperature EPR spectra measurements have been performed to determine the presence of paramagnetic defects in the crystal. The spectra at selected orientations are shown in Fig. 2. Resonances of varying intensities have been observed in a broad spectral range and exhibit a pronounced dependence on the crystal orientation relative to external field direction. Such EPR spectra are typical for high spin S transition metal or rare earth ion impurities situated in strong crystal fields of the lattice. Judging from the number of lines and their relative intensities, the lack of obvious hyperfine (HF) structure and the fact the spectra have been recorded at room temperature, the most likely candidates are Fe^{3+} ($S = 5/2$) and Gd^{3+} ($S = 7/2$). A qualitatively similar angle-dependent behaviour has been reported for low symmetry Gd^{3+} centres in different hosts [31–33]. If this is the case here, then all of the resonances could be accounted for with a single $S = 7/2$ system implying

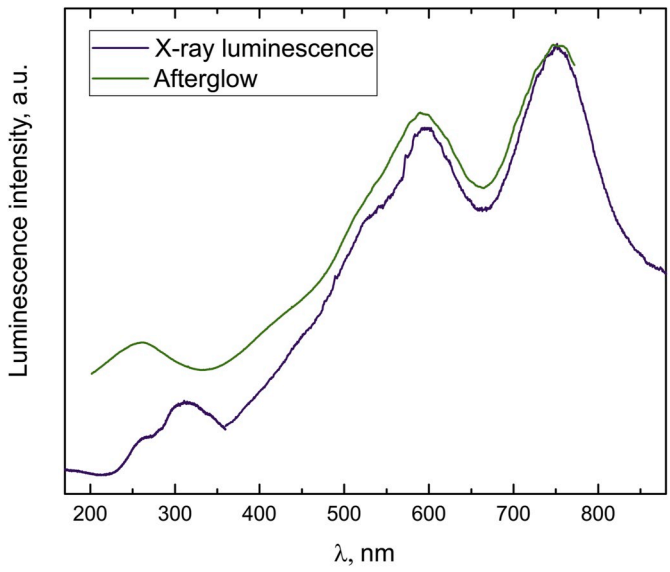

Fig. 3. Comparison of X-ray luminescence and RL spectra of BaY_2F_8.

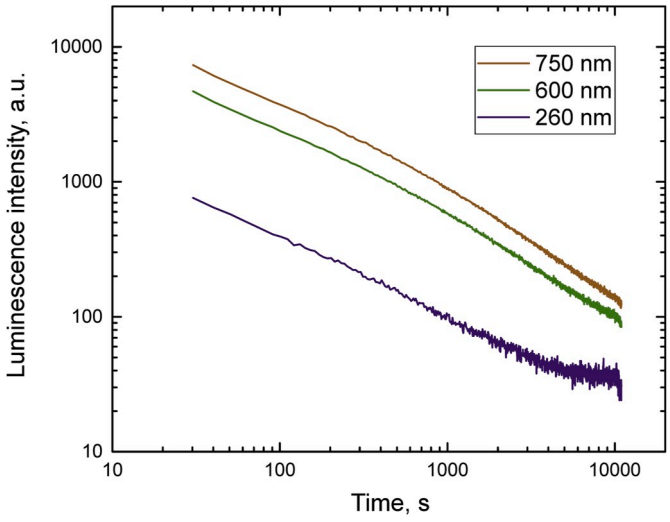

Fig. 4. Decay kinetics on a double logarithmic scale of the RL spectra shown in Fig. 3.

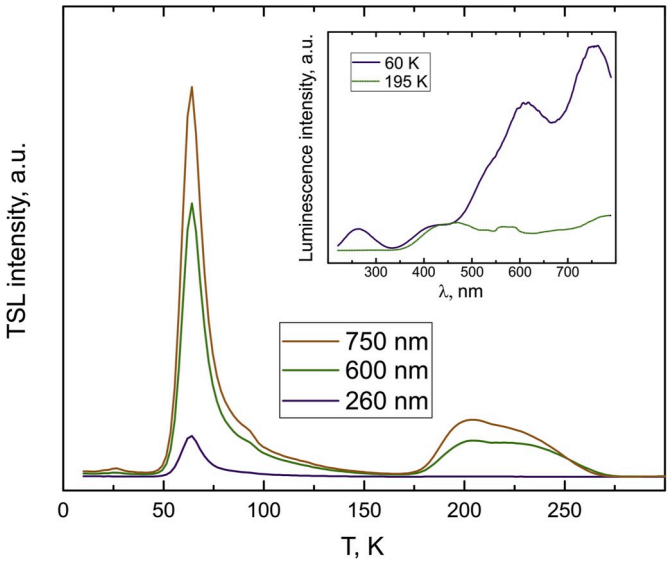

Fig. 5. TSL glow curves obtained for different luminescence wavelengths. The inset shows TSL spectra measured at 60 K and 195 K.

one unique position for the Gd^{3+} ion in the BaY_2F_8 lattice. The concentration of the impurities is below the detection limit of X-ray fluorescence analysis (≈10 ppm). Additionally, a weaker signal with a more complicated structure, which is demonstrated in the inset of Fig. 2, can be resolved in the EPR spectra. The signal has been assigned to Mn^{2+} impurities based on the six-component HF structure pattern at ≈ 0.2 T. Each of the hyperfine lines is further split due electron spin interaction with surrounding F^- nuclei as is typical for manganese paramagnetic centres in fluoride crystals [34].

Consequently, the superposition of several EPR signals in the $g \approx 2$ region inhibits a straightforward analysis of radiation-induced defects in the crystal with the conventional EPR technique. Therefore, in this study we attempt an optical detection of paramagnetic centres, where the resonance signals are detected directly on a selected luminescence band thus eliminating contributions from impurity ions.

3.2. RL

X-ray luminescence and RL spectra are shown in Fig. 3. Both spectra

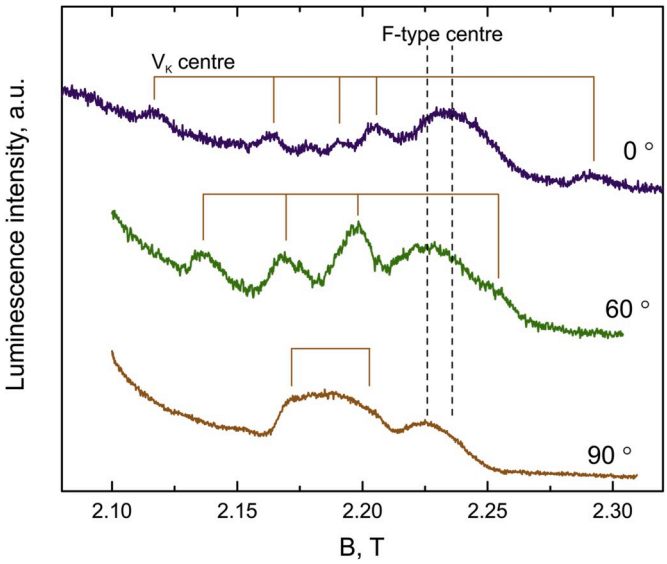

Fig. 6. Decay of the **integral** RL signal intensity as a function of external magnetic field at applied 62 GHz microwaves. The RL-EPR lines appear at resonance fields, which depend on the crystal orientation relative to magnetic field.

in the range of 350–800 nm are similar in shape. This allows to conclude that X-ray luminescence is caused by recombination processes, which involve electron and hole trap centres.

RL decay kinetics in the 260 nm, 600 nm and 750 nm bands, which are presented in Fig. 4, are rather linear in double-logarithmic coordinates. A linear decay in double-logarithmic coordinates is characteristic for the tunnelling recombination process between spatially correlated electron trap centre and hole trap centre pairs [35,36], however, the measurement time must well exceed the irradiation time [37]. In our case the irradiation time was 20 min, which means that up to ≈1000 s some "memory" effect of the irradiation time still persists.

In order to validity the hypothesis of the tunnelling luminescence nature of the RL decay at low temperature, TSL measurements were performed. The results are shown in Fig. 5.

The first major maximum is observed at 65 K. As the RL spectra were acquired at 10 K or below (in the RL-EPR experiments), thermal stimulation effects can be excluded and at 10 K only tunnelling luminescence is expected. The TSL spectrum in the inset of Fig. 5 Is similar to the afterglow spectrum in Fig. 3, which means that the 65 K TSL peak is determined by the recombination of the same electron and hole centres. The TSL spectrum of the 195 K maximum differs substantially, therefore it involves other recombination processes.

3.3. RL-EPR

RL is a process, which involves spatially separated electron and hole trap centres. When an electron tunnelling occurs, it recombines with a hole and a quantum of light is emitted. In the presence of external magnetic field the spins of electron and hole centres are oriented along the direction of the field. For a recombination process, which requires a singlet state, the alignment of spins decreases the probability of recombination, thus a diminishing RL signal intensity is expected as a function of the field magnitude [25,38]. In RL-EPR experiments microwaves are continuously applied during the sweep of magnetic field. At particular field values the EPR resonance condition is met and reorientation of the electron or the hole centre spin occurs. At that moment the recombination process becomes allowed and a RL signal intensity increase can be observed. From the analysis of angle-dependent behaviour of RL-EPR resonance positions in single crystals a direct identification of the defects responsible for the RL signal is possible.

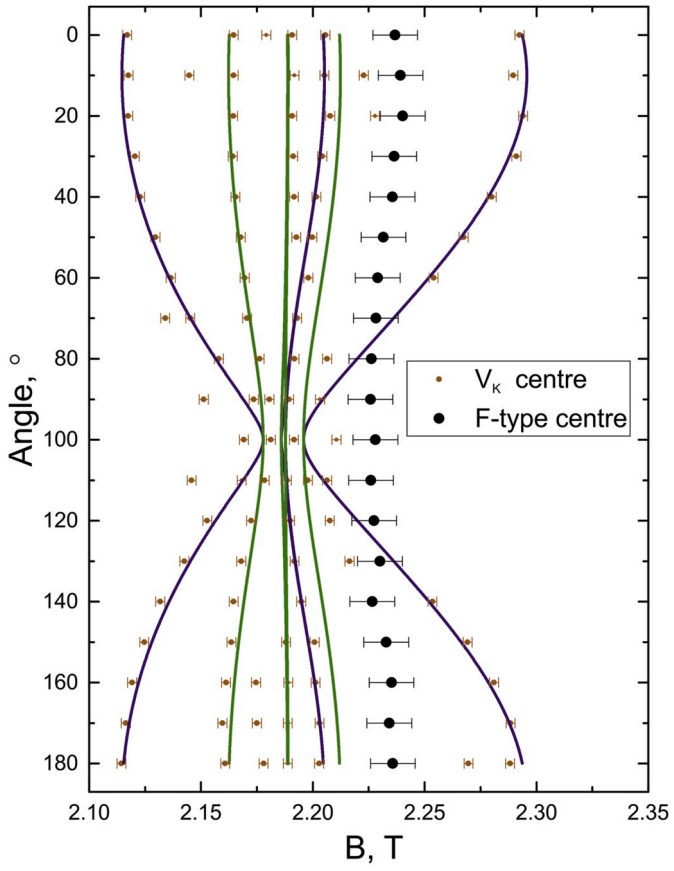

Fig. 7. Angular dependences of the RL-EPR spectra. Simulation results are represented as curves, where the different colours correspond to two distinct centre orientations as shown in Table 1.

RL-EPR spectra at selected crystal orientations relative to the external magnetic field are shown in Fig. 6. The resonance band positions could be estimated and represented as an RL-EPR angular dependence in one plane. Angular variations of the RL-EPR spectra resonance positions under a 180° crystal rotation with a 10° step are presented in Fig. 7. The "0°" spectrum has been chosen as the orientation with the maximum splitting, the uncertainty of the rotation angle has been estimated to be ±1°. The uncertainties of the resonance positions have been evaluated on the basis on the RL-EPR peak linewidths.

The RL-EPR spectra consist of a relatively broad and isotropic line at $g \approx 1.98$ and a set of highly anisotropic resonances. A negative shift from the free electron g value suggests that it is an electron (F) type centre [39]. A likely candidate is the F-centre – an electron trapped at an anion vacancy. In this case the significant broadening could be explained by the unresolved superhyperfine structure due to interaction with 100% abundant ^{19}F nuclei with nuclear spin $I = 1/2$ within the first coordination sphere of the centre.

The nature of the angle-dependent lines is very similar to V_K centres reported in fluoride crystals [40–42]. The V_K centre, also known as the self-trapped hole, can be considered as a F_2^- molecular ion with the hole distributed across the two ions. This causes a highly anisotropic HF interaction of the $S = 1/2$ system with the adjacent two ^{19}F nuclei. As a result, splitting in the EPR spectrum is relatively large, when the molecular axis is parallel to external magnetic field and an order of magnitude smaller – when perpendicular to it.

The resonance positions can be approximated by an axial spin-Hamiltonian (SH):

$$\widehat{H} = \mu_B \vec{B} \tilde{g} \widehat{\vec{S}} + \sum_{i=1}^{2} \widehat{\vec{S}} \tilde{A} \widehat{\vec{I}_i} \quad (1)$$

Table 1
Euler angles of centre orientations used in simulations.

Centre	α, °	β, °	γ, °
1	10	80	0
2	10	15	0

Table 2
A survey of SH parameters for self-trapped hole centres in different fluoride hosts. $g_\perp$ and $A_\perp$ taken as the average of x and y components of the respective tensor, if presented.

Crystal	$g_\parallel$	$g_\perp$	$A_\parallel$, MHz	$A_\perp$, MHz	Reference
BaY_2F_8	2.007	2.023	2584	255	This work
LiF	2.0031	2.0230	2486	165	[40]
NaF	2.0014	2.0220	2514	132	[41]
KF	2.0020	2.0214	2545	84	[41]
CaF_2	2.001	2.020	2520	137	[45]
SrF_2	2.0024	2.0192	2517	131	[46]
BaF_2	2.001	2.012	2510	121	[47]
$KMgF_3$	2.0024	2.0210	2476	159	[48]
$CsCdF_3$	2.0008	2.020	2482		[49]
$RbCaF_3$	2.0030	2.023	2567	28	[50]
$LiBaF_3$	2.002	2.024	2520	200	[51]
$LiYF_4$	2.0019	2.021	2550	22	[52]
$CsNaYF_4$	2.0028	2.0227	2460	207	[53]

where μ_B is the Bohr magneton; $\tilde{g}$ – the g-tensor; $\tilde{A}$ – the HF interaction tensor. For simulations two centre orientations (distinguished by the different colour simulation curves in Fig. 7) with identical SH parameters were chosen with the Euler angles specified in Table 1. The three Euler angles characterize the rotation of the coordinate system for each centre relative to laboratory coordinate system: α denotes rotation around the z-axis, whereas β – around the new y_1-axis [43]. The orientations were chosen by a trial and error approach to achieve the best fit to experimental points. The determined SH parameters are $g_\parallel = 2.007 \pm 0.005$; $g_\perp = 2.023 \pm 0.005$; $A_\parallel = 2584 \pm 50$ MHz and $A_\perp = 255 \pm 50$ MHz. Average deviation of the calculated resonance positions from the experimental data points is 2.9 mT. Due to the specifics of the RL-EPR detection technique uncertainties in the determined values of SH parameters are relatively large in comparison to the conventional CW-EPR.

A comparison with SH parameter values in other fluorides given in Table 2 further evidences that the observed signals belong to a self-trapped hole. Defect assignment to a specific location in the crystal lattice is problematic due to unknown rotation axis during the experiments as well as the complicated crystal structure shown in Fig. 1, especially, if viewed from the position of F^- sites. Given the number of possible F–F pair directions in the crystal structure, it is surprising that the majority of RL-EPR spectra positions could be simulated by just two such molecule orientations. Indeed, in fluorides with a complicated crystal structure overlapping EPR signals from several self-trapped hole centres are typical. For example, in K_2YF_5 five types of F_2^- centres have been reported [44]. The selective observation of a single centre in the current work could be explained by the detection of EPR signals, which are responsible for recombination processes at 4.2 K. Thus, the presence of other V_K centres, which are stable at this temperature, cannot be excluded. A more precise SH parameter determination and defect structure association with the crystal structure would, of course, benefit from variable temperature CW-EPR and ENDOR studies.

Without an applied magnetic field the decay of RL follows the time dependence shown in Fig. 4. Generally, in the presence of magnetic field the RL intensity has an additional decrease, if the recombination process between the donor electron and acceptor hole occurs through the singlet state [25,35]. Therefore, the amplitude of the RL-EPR effect could have been affected by the time which had elapsed after the switching off the X-ray irradiation source. However, the positions of the RL-EPR lines are affected only by the nature of donor and acceptor centres, which is the

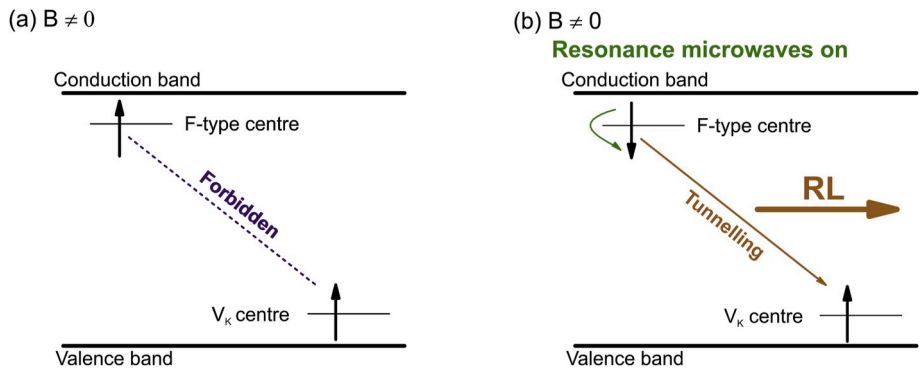

Fig. 8. A simplified diagram explaining the mechanism of afterglow in BaY_2F_8 and the principle of RL-EPR **experiment**: (a) represents spin alignment in the presence of external magnetic field; (b) the resonance condition, when the energy of microwaves is equal to the energy difference between the spin states of the F-type centre.

primary focus of the present study.

Measurements of RL-EPR spectra with different optical band-pass filters (in the range 200–350 nm and 350–650 nm) showed no changes in the shape of the RL-EPR spectrum. RL-EPR measurements with the edge filter for wavelengths longer than 650 nm showed diminishing RL-EPR response, mainly due to the reduced sensitivity in the red region of the RL-EPR setup. As a result, we can conclude that the whole spectrum in the 250–650 nm range is caused by the recombination process of the same type of electron and hole trap centres. However, it is also possible that in the BaY_2F_8 crystal structure there is more than one F-type centre, which could lead to the appearance of more than one RL band in the 250–650 nm range.

A summary of the low temperature afterglow mechanism in BaY_2F_8 and the RL-EPR detection technique is given in Fig. 8. Anion vacancies are inevitably present in the as-grown BaY_2F_8 crystal. During irradiation with X-rays electrons are removed from some of the F^- ions. The resulting electron deficiencies are shared equally by two neighbouring anions creating V_K centres, while the excess electrons are localized at anion vacancies as F-type centres. The electrons from the F-type centres recombine with the holes of the V_K centres via the tunnelling phenomenon, which is observed in the form of RL. In the presence of external magnetic field the process is suppressed due to alignment of electron and hole spins, however it can be restored by the application of resonant microwaves. For the 62 GHz microwaves used here the spin-flip transitions of the F-type centre are achieved at $B \approx 2.23$ T ($g = 1.98$), which is visible in Fig. 6 as the RL intensity increase at the specified field value. Similarly, the resonance condition can be achieved also for the V_K centre, and for a constant microwave frequency experiment it is ensured at different magnetic field values as determined by the SH parameters in this study.

4. Conclusions

A long-lasting afterglow has been observed in BaY_2F_8 crystal after irradiation with X-rays at low temperature (4.2 K). Resonance signals at $g \approx 2$ with a pronounced angular dependence appear in RL-EPR spectra. In spectral simulations we have used a model with $S = 1/2$ and anisotropic interaction with two nuclear spins with $I = 1/2$. The determined hyperfine structure parameter numerical values have a good agreement with self-trapped hole centres (V_K centres) in other fluorides. The V_K centre recombines with a F-type electron trap centre and is responsible for broad bands in the 250–650 nm range of the RL spectrum.

Declaration of competing interest

The authors declare that they have no known competing financial interests or personal relationships that could have appeared to influence the work reported in this paper.

CRediT authorship contribution statement

Andris Antuzevics: Conceptualization, Formal analysis, Investigation, Writing - original draft, Writing - review & editing, Visualization, Project administration. **Andris Fedotovs:** Software, Methodology, Investigation. **Dzintars Berzins:** Methodology, Investigation. **Uldis Rogulis:** Conceptualization, Validation, Writing - original draft, Writing - review & editing, Supervision, Funding acquisition. **Krisjanis Auzins:** Methodology, Investigation. **Aleksejs Zolotarjovs:** Methodology, Investigation. **Sonia Licia Baldochi:** Resources.

Acknowledgements

This research is funded by the Latvian Council of Science, project "Novel transparent nanocomposite oxyfluoride materials for optical applications", project No. LZP-2018/1–0335. The crystal growth research was funded by the CNPq(Brazil), project NO 421581/2016–6.

References

[1] L.F. Johnson, H.J. Guggenheim, Infrared-pumped visible laser, Appl. Phys. Lett. 19 (1971) 44–47, https://doi.org/10.1063/1.1653816.
[2] L.F. Johnson, H.J. Guggenheim, New laser lines in the visible from Er^{3+} ions in BaY_2F_8, Appl. Phys. Lett. 20 (1972) 474–477, https://doi.org/10.1063/1.1654022.
[3] V.I. Baryshnikov, S.N. Vesnina, A.A. Shestakov, Efficiency of the generation and self-addition of laser line frequencies upon the diode pumping of Er:BaY_2F_8 crystals, Bull. Russ. Acad. Sci. Phys. 81 (2017) 1115–1118, https://doi.org/10.3103/s1062873817090040.
[4] L.F. Johnson, H.J. Guggenheim, Laser emission at 3 μ from Dy^{3+} in BaY_2F_8, Appl. Phys. Lett. 23 (1973) 96–98, https://doi.org/10.1063/1.1654822.
[5] R.A. McFarlane, Upconversion laser in BaY_2F_8:Er 5% pumped by ground-state and excited-state absorption, J. Opt. Soc. Am. B 11 (1994) 871, https://doi.org/10.1364/josab.11.000871.
[6] R.J. Thrash, L.F. Johnson, Upconversion laser emission from Yb^{3+}-sensitized Tm^{3+} in BaY_2F_8, J. Opt. Soc. Am. B 11 (1994) 881–885.
[7] E. Osiac, E. Heumann, G. Huber, S. Kück, E. Sani, A. Toncelli, M. Tonelli, Orange and red upconversion laser pumped by an avalanche mechanism in Pr^{3+}, Yb^{3+}: BaY_2F_8,, Appl. Phys. Lett. 82 (2003) 3832–3834, https://doi.org/10.1063/1.1579561.
[8] F. Cornacchia, D. Parisi, C. Bernardini, A. Toncelli, M. Tonelli, Efficient, diode-pumped Tm^{3+}:BaY_2F_8 vibronic laser, Optic Express 12 (2004) papers2://publication/uuid/A2523489-8D04-4D1E-AF40-1CBE92F9ABB7.
[9] G. Galzerano, F. Cornacchia, D. Parisi, A. Toncelli, M. Tonelli, P. Laporta, Widely tunable 1.94-μm Tm:BaY_2F_8 laser, Opt. Lett. 30 (2005) 854, https://doi.org/10.1364/OL.30.000854.
[10] D. Pabœuf, O. Mhibik, F. Bretenaker, P. Goldner, D. Parisi, M. Tonelli, Diode-pumped Pr:BaY_2F_8 continuous-wave orange laser, Opt. Lett. 36 (2011) 280–282, https://doi.org/10.1364/OL.36.000280.
[11] A.A. Kaminskii, O. Lux, J. Hanuza, H. Rhee, H.J. Eichler, J. Zhang, D. Tang, D. Shen, H. Yu, J. Wang, H. Yoneda, A. Shirakawa, Monoclinic β-BaY_2F_8 —a novel crystal simultaneously active for SRS and Ln^{3+} -ion lasing, Laser Phys. 25 (2015), 015801, https://doi.org/10.1088/1054-660X/25/1/015801.
[12] J. Pejchal, M. Nikl, K. Fukuda, N. Kawaguchi, T. Yanagida, Y. Yokota, A. Yoshikawa, V. Babin, Doubly doped BaY_2F_8:Er,Nd VUV scintillator, Radiat. Meas. 45 (2010) 265–267, https://doi.org/10.1016/j.radmeas.2009.10.017.
[13] S. Kurosawa, T. Yanagida, J. Pejchal, K. Fukuda, N. Kawaguchi, S. Ishizu, T. Suyama, M. Nakagawa, Y. Yokota, M. Nikl, A. Yoshikawa, Evaluation of Nd:

BaY_2F_8 for VUV scintillator, Radiat. Meas. 55 (2013) 108–111, https://doi.org/10.1016/j.radmeas.2013.01.011.
[14] S. Bigotta, A. Di Lieto, D. Parisi, A. Toncelli, M. Tonelli, Single fluoride crystals as materials for laser cooling applications, in: Laser Cool. Solids, 2007, p. 64610E, https://doi.org/10.1117/12.701989.
[15] A. Boccolini, R. Faoro, E. Favilla, S. Veronesi, M. Tonelli, BaY_2F_8 doped with Er^{3+}: An upconverter material for photovoltaic application, J. Appl. Phys. 114 (2013), https://doi.org/10.1063/1.4817171.
[16] S. Fischer, E. Favilla, M. Tonelli, J.C. Goldschmidt, Record efficient upconverter solar cell devices with optimized bifacial silicon solar cells and monocrystalline BaY_2F_8:30% Er^{3+} upconverter, Sol. Energy Mater. Sol. Cells 136 (2015) 127–134, https://doi.org/10.1016/j.solmat.2014.12.023.
[17] A. Boccolini, E. Favilla, M. Tonelli, B.S. Richards, R.R. Thomson, Highly efficient upconversion in Er^{3+} doped BaY_2F_8 single crystals: dependence of quantum yield on excitation wavelength and thickness, Optic Express 23 (2015) A903, https://doi.org/10.1364/OE.23.00A903.
[18] G.B. Nair, A. Kumar, H.C. Swart, S.J. Dhoble, Facile precipitation synthesis of green-emitting BaY_2F_8:Yb^{3+}, Ho^{3+} upconverting phosphor, Ceram. Int. (2019), https://doi.org/10.1016/j.ceramint.2019.04.127, 0–1.
[19] L.H. Guilbert, J.Y. Gesland, A. Bulou, Structure and Raman spectroscopy of czochralski-grown barium yttrium and barium ytterbium fluorides crystals, Mater. Res. Bull. 28 (1993) 923–930, https://doi.org/10.1016/0025-5408(93)90039-G.
[20] S.M. Kaczmarek, G. Leniec, J. Typek, G. Boulon, A. Bensalah, Optical and EPR study of BaY_2F_8 single crystals doped with Yb, J. Lumin. 129 (2009) 1568–1574, https://doi.org/10.1016/j.jlumin.2009.04.063.
[21] N. Magnani, G. Amoretti, A. Baraldi, R. Capelletti, Crystal-field and superposition model analysis of R^{3+}:BaY_2F_8 (R = Er, Dy, Nd), Eur. Phys. J. B. 29 (2002) 79–84, https://doi.org/10.1140/epjb/e2002-00264-0.
[22] N. Magnani, G. Amoretti, A. Baraldi, R. Capelletti, Superposition-model analysis of rare-earth doped BaY_2F_8, Radiat. Eff. Defect Solid 157 (2002) 921–926.
[23] Z. Kowalski, S.M. Kaczmarek, K. Brylew, W. Drozdowski, Radioluminescence as a function of temperature and low temperature thermoluminescence of BaY_2F_8:Ce and BaY_2F_8:Nd crystals, Opt. Mater. (Amst). 59 (2016) 145–149, https://doi.org/10.1016/j.optmat.2015.12.047.
[24] A.B. Andrade, G.F. Giordano, Z.S. Macedo, S.L. Baldochi, E.G. Yukihara, M.E. G. Valerio, VUV excited luminescence and thermoluminescence investigation on Er^{3+}- or Pr^{3+}-doped BaY_2F_8 single crystals, Opt. Mater. (Amst). 90 (2019) 238–243, https://doi.org/10.1016/j.optmat.2019.02.044.
[25] N.G. Romanov, Y.P. Veshchunov, V.A. Vetrov, P.G. Baranov, Application of tunneling recombination afterglow for EPR optical detection of recombining centres in ionic crystals, Phys. Status Solidi 107 (1981) K119–K124, https://doi.org/10.1002/pssb.2221070255.
[26] K. Momma, F. Izumi, VESTA 3 for three-dimensional visualization of crystal, volumetric and morphology data, J. Appl. Crystallogr. 44 (2011) 1272–1276, https://doi.org/10.1107/S0021889811038970.
[27] S. Gražulis, A. Daškevič, A. Merkys, D. Chateigner, L. Lutterotti, M. Quirós, N. R. Serebryanaya, P. Moeck, R.T. Downs, A. Le Bail, Crystallography Open Database (COD): An open-access collection of crystal structures and platform for world-wide collaboration, Nucleic Acids Res. 40 (2012) 420–427, https://doi.org/10.1093/nar/gkr900.
[28] A.C.S. De Mello, A.B. Andrade, G.H.G. Nakamura, S.L. Baldochi, M.E.G. Valerio, Luminescence properties of Er^{3+} and Tm^{3+} doped BaY_2F_8, J. Lumin. 138 (2013) 19–24, https://doi.org/10.1016/j.jlumin.2012.12.001.
[29] V. Grachev, Visual-EPR, (n.d.). www.visual-epr.com.
[30] V.G. Grachev, Y.G. Semenov, Methods of computer treatment of EPR and ENDOR spectra, Radiospectroscopy (1983) 163–171.
[31] G. Amoretti, D.C. Giori, V. Varacca, EPR of Gd^{3+} in a single crystal of thorium disulfide (ThS_2), Z. Naturforsch. 36a (1981) 1163–1168.
[32] N.V. Cherney, V.A. Nadolinnyi, A.A. Pavlyuk, ESR of Gd^{3+} ions in potassium yttrium tungstate, J. Struct. Chem. 46 (2006) 619–625, https://doi.org/10.1007/s10947-006-0179-x.
[33] S.K. Misra, S.I. Andronenko, A variable-temperature X-band EPR study of the Gd^{3+} ion in a $La_2Si_2O_7$ crystal characterized by monoclinic site symmetry, Appl. Magn. Reson. 32 (2007) 377–384, https://doi.org/10.1007/s00723-007-0020-5.
[34] W. Gehlhoff, W. Ulrici, Transition metal ions in crystals with the fluorite structure, Phys. Status Solidi 102 (1980) 11–59, https://doi.org/10.1002/pssb.2221020102.
[35] T. Tashiro, S. Takeuchi, M. Saidoh, N. Itoh, Luminescence induced by tunnelling recombination between neutral silver atoms and V_k centres in alkali halides, Phys. Status Solidi 92 (1979) 611–618, https://doi.org/10.1002/pssb.2220920234.
[36] V.J. Grabovskis, I.K. Vitols, Tunneling recombination luminescence in KBr and KCl, J. Lumin. 20 (1979) 337–342.
[37] D.E. Aboltin, V.J. Grabovskis, A.R. Kangro, C. Lushchik, A.A. O'Konnel-Bronin, I. K. Vitol, V.E. Zirap, Thermally stimulated and tunneling luminescence and frenkel defect recombination in KCl and KBr at 4.2 to 77 K, Phys. Status Solidi 47 (1978) 667–675, https://doi.org/10.1002/pssa.2210470239.
[38] P.G. Baranov, M.F. Bulanyi, V.A. Vetrov, N.G. Romanov, Optically detected in ESR in ZnS and ZnS:Mn crystals, JETP Lett 38 (1983).
[39] A.S. Marfunin, Spectroscopy, Luminescence and Radiation Centers in Minerals, Springer Science & Business Media, 2012.
[40] T.O. Woodruff, W. Känzig, Paramagnetic resonance absorption of a V center in LiF, J. Phys. Chem. Solid. 5 (1958) 268–287, https://doi.org/10.1016/0022-3697(58)90030-1.
[41] C.E. Bailey, Hyperfine structure of v_k centers in Alkali fluoride crystals, Phys. Rev. 136 (1964) 1960–1965, https://doi.org/10.1103/PhysRev.136.A1311.
[42] R.F. Marzke, R.L. Mieher, Electron-nuclear double resonance of the self-trapped hole in CaF_2 and BaF_2, Phys. Rev. 182 (1969) 453–458, https://doi.org/10.1103/PhysRev.182.453.
[43] D.A. Varshalovich, A.N. Moskalev, V.K. Khersonskii, Elements of vector and tensor theory, in: Quantum Theory of Angular Momentum, 1988, https://doi.org/10.1142/9789814415491_0002.
[44] D.G. Zverev, H. Vrielinck, E. Goovaerts, F. Callens, Electron paramagnetic resonance study of rare-earth related centres in K_2YF_5:Tb^{3+} thermoluminescence phosphors, Opt. Mater. (Amst). 33 (2011) 865–871, https://doi.org/10.1016/j.optmat.2011.01.011.
[45] W. Hayes, J.W. Twidell, The self-trapped hole in CaF_2, Proc. Phys. Soc. 79 (1962) 1295–1296, https://doi.org/10.1088/0370-1328/79/6/126.
[46] R. Gazzinelli, G.M. Ribeiro, M.L. de Siqueira, ESR and endor studies of the V_K center in SrF_2, Solid State Commun. 13 (1973) 1131–1134, https://doi.org/10.1016/0038-1098(73)90548-6.
[47] Y. Kazumata, Self-trapped holes in neutron irradiated CaF_2 and BaF_2 crystals, Phys. Status Solidi 26 (1968) K119–K122, https://doi.org/10.1002/pssb.19680260251.
[48] T.P.P. Hall, The structure of the self-trapped hole in $KMgF_3$, Br. J. Appl. Phys. 17 (1966) 1011–1018, https://doi.org/10.1088/0508-3443/17/8/306.
[49] J.J. Rousseau, J.C. Fayet, Influence of the crystal field on bent configuration of V_K centres in AMF_3 compounds, Phys. Status Solidi 77 (1976) 195–201, https://doi.org/10.1002/pssb.2220770117.
[50] L.E. Halliburton, E. Sonder, V_K centers in $RbCaF_3$: lattice distortion in the tetragonal phase, Solid State Commun. 21 (1977) 445–447, https://doi.org/10.1016/0038-1098(77)91371-0.
[51] I. Tale, M. Springis, U. Rogulis, V. Ogorodnik, P. Kulis, V. Tale, A. Veispals, H. J. Fitting, Self-trapped holes and recombination luminescence in $LiBaF_3$ crystals, Radiat. Meas. 33 (2001) 751–754, https://doi.org/10.1016/S1350-4487(01)00096-8.
[52] M. Herget, A. Hofstaetter, A. Scharmann, EPR of the F_2^- center in $LiYF_4$, Phys. Status Solidi 127 (1985) K83–K87, https://doi.org/10.1002/pssb.2221270165.
[53] T. Pawlik, J.-M. Spaeth, Investigation of radiation-induced defects in Cs_2NaYF_6, Phys. Status Solidi 203 (1997) 43–52, https://doi.org/10.1002/1521-3951(199708)202:2<993::aid-pssb993>3.0.co;2-t.

Institute of Solid State Physics, University of Latvia as the Center of Excellence has received funding from the European Union's Horizon 2020 Framework Programme H2020-WIDESPREAD-01-2016-2017-TeamingPhase2 under grant agreement No. 739508, project CAMART²